

N -body simulation of a clumpy torus: application to active galactic nuclei

E.Yu. Bannikova^{1,2*}, V.G. Vakulik^{1,2†} and A.V. Sergeev^{1,2}

¹ Institute of Radio Astronomy of the National Academy of Sciences of Ukraine, Krasnoznamennaya 4, 61022 Kharkov, Ukraine

² Karazin Kharkov National University, Svobody Sq. 4, 61022 Kharkov, Ukraine

Accepted 2012 April 25 . Received 2012 April 12 ; in original form 2012 January 18

ABSTRACT

The gravitational properties of a torus are investigated. It is shown that a torus can be formed from test particles orbiting in the gravitational field of a central mass. In this case, a toroidal distribution is achieved because of the significant spread of inclinations and eccentricities of the orbits. To investigate the self-gravity of the torus we consider the N -body problem for a torus located in the gravitational field of a central mass. It is shown that in the equilibrium state the cross-section of the torus is oval with a Gaussian density distribution. The dependence of the obscuring efficiency on torus inclination is found.

Key words: gravitation - galaxies: active -galaxies: nuclei - galaxies: Seyfert

1 INTRODUCTION

Obscuring dusty tori are important structural elements of Active Galactic Nuclei (AGN). In the framework of the unified scheme, the differences in the AGN are explained by the orientation of the torus relative to an observer (Antonucci 1993; Urry & Padovani 1995). Full obscuration of the central engine (black hole + accretion disk) and the Broad Line Region (BLR) is realized when the torus is seen edge-on. In this case, only narrow emission lines are detected in spectrum, and this type of AGN is called 'type 2'. In contrast, if the torus is inclined at some angle to the line of sight, the emission from the accretion disk and BLR can be seen to the observer ('type 1'). Following from the statistical data, the torus must be geometrically thick in order to explain the observed properties of Seyfert galaxies (Osterbrock & Shaw 1988; Schmitt et al. 2001).

The first direct evidence for the existence of a compact structure in the nucleus of Sy2 galaxy NGC 1068 was found with help of near-infrared bispectrum speckle interferometry (Wittkowski et al. 1998; Weigelt et al. 2004) and speckle interferometry (Weinberger, Neugebauer & Matthews 1999). Subsequently, observations of NGC 1068 using VLTI/MIDI in the infrared band ($10\mu m$) allowed, for the first time, a spatial distribution of temperature in the torus to be obtained (Jaffe et al. 2004). It was discovered that the torus has two components: a hot compact component ($T > 800K$) and a warm component ($T = 300K$). The hot component is about 1.35 parsec long and 0.45 parsec thick; the size of the

warm component is $3 \times 4pc$ (Raban et al. 2009). Thus, the observations confirmed a substantial geometrical thickness of the torus: the minor-to-major radius ratio r_0 is about 0.7. It is suggested that the hot component discovered by Jaffe et al. (2004) is the inner funnel of the obscuring torus heated by radiation of the accretion disc, while the warm component is the torus body itself (Schartmann et al. 2005, Dullemond & Bommert 2005, Raban et al. 2009).

The mass of the obscuring torus can be estimated from the rotation curve obtained from observations of maser emission. Greenhill et al. (1996) obtained VLBI synthesis images of the H_2O maser emission from the central region of NGC 1068. They found a good fit to the data by assuming a non-Keplerian rotation curve of the form $V \propto r^{-0.31}$ on spatial scales above 0.6 pc. The deviation of the rotation curve from Keplerian may be a result of the influence of the self-gravitation of the torus (Greenhill et al. 1996). It turns out that in the case of NGC 1068, the torus mass could be comparable to the mass of the central black hole (Hur e 2002; Lodato & Bertin 2003).

One of the problems concerning obscuring tori is how they stand up against gravity. To explain the required geometrical thickness of a torus, the magnitude of random speeds in the vertical direction must be about: $\Delta V_z/V_{orb} \approx r_0$. Krolik & Begelman (1988) noted that if this motion is thermal, the corresponding temperature ($\sim 10^6 K$) would be far too hot for dust to survive. Therefore it was assumed that the torus material is distributed in clouds. To support cloud motions against losses by collisions, orbital shear energy can be randomized if magnetic fields make the clouds sufficiently elastic (Krolik & Begelman 1988). However, the required magnetic fields have not been

* E-mail: bannikova@astron.kharkov.ua

† Deceased

detected. Pier & Krolik (1992) suggested a mechanism in which a geometrically thick torus can be explained by the influence of the infrared radiation pressure. Krolik (2007) obtained an explicit solution of hydrostatic equilibrium within a torus on the assumption of a continuous medium. In the framework of this solution it was shown that the infrared radiation pressure can support geometrically thick structures in AGN. In this case, the density distribution in torus cross-section reaches its maximum near the inner edge of the torus with a subsequent decrease to the outer edge. Schartmann et al. (2005, 2008) suggested a turbulent torus model in which the dusty clouds are ejected by stars and take over the stellar velocity dispersion. In this model, the torus is considered as a continuous medium and the turbulent motions lead only to a weak stabilization against gravity (Schartmann et al. 2010). Starburst-driven tori were investigated with the help of a hydrodynamical simulation of the interstellar medium by Wada & Norman (2002) and Wada, Papadopoulos & Spaans (2009). The other idea is the presence of a dipole vortex motion in the torus that can support its geometrical thickness (Bannikova & Kontorovich 2007). There are also models in which the obscuring region is produced by a hydromagnetic wind (Königl & Kartje 1994; Elitzur & Shlosman 2006). The main problem of these models is the unknown origin of the large-scale magnetic field needed to support such winds. An alternative to models of wind scenarios is that of outflows driven by infrared radiation pressure on dust (Dorodnitsyn, Bisnovatyi-Kogan & Kallman 2011, 2012).

In hydrodynamic models the torus is considered as a continuous medium, and hence the motion of matter (the clouds) is parallel to the torus plane of symmetry. In this case, gravity tends to compress the torus into a disk, and therefore the substantial forces are required to work against gravity. In this paper we consider discrete clouds moving in the gravitational field of the central mass. In this case, the orbital plane of each cloud passes through the central mass. The clouds form a Keplerian disc if their orbits lie in one plane. The toroidal structure can be formed by clouds moving in orbits of different inclinations and eccentricities. Such orbits are similar to those of stars moving around the supermassive black hole in the Galactic centre (Ghez et al. 2005). Note that recent observations have detected in this region a dusty cloud, which also moves in a very elongated orbit with large inclination (Gillessen et al. 2012).

In this paper we investigate the gravitational properties of a torus composed of clouds moving in orbits with different inclinations and eccentricities. We start with an idealized case, considering clouds in approximation of test particles moving on Keplerian orbits in the gravitational field of the central mass (Section 2). In Section 3 we considered the problem of test particle motion in the inner gravitational potential of a homogeneous circular torus and central mass. In Section 4, the N -body problem for a torus located in the gravitational field of a central mass is investigated. The equilibrium cross-section of self-gravitating torus is found, and its evolution over long times is analyzed. The obtained results are used for the interpretation of the observed features of the obscuring tori in AGN (Section 5).

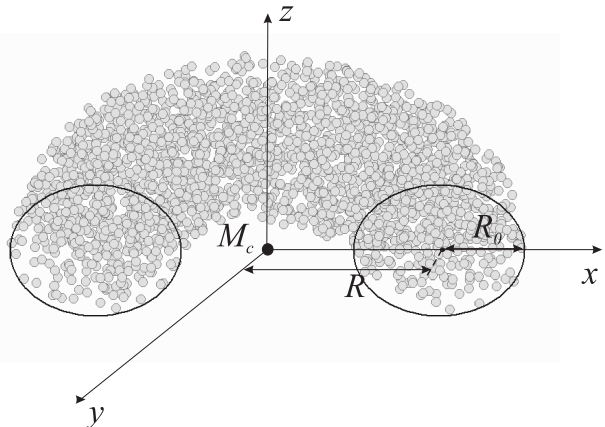


Figure 1. The scheme of the torus, which consists of particles orbiting in gravitational field of a central mass M_c .

2 KEPLERIAN TORUS

Let us consider the problem of test particles motion in the gravitational field of a central mass M_c (Fig.1). This is a two-body problem for each particle. We can impose conditions on the orbital elements such that the particles form a toroidal structure. In this case, a substantial geometrical thickness of the torus can be reached owing to the significant scatter of inclinations and eccentricities of the particles orbits. Because particles move on unperturbed (Keplerian) orbits, we will call a torus formed in this way a "Keplerian torus".

To create a Keplerian torus we impose the following conditions:

- a) the shape of the cross-section of the torus must be close to circular or elliptic;
- b) the spatial distribution of particles in the torus must be close to homogeneous;
- c) the orbits of particles in the comoving system of coordinates must be nested. This condition allows us to avoid intersections of orbits and hence collisions between particles.¹

The torus is characterized by two geometrical parameters: major R and minor R_0 radii (Fig. 1). It is convenient to introduce the geometrical parameter $r_0 = R_0/R$. To ensure a quasi-circular cross-section of the torus, we should choose the semi-major axes of the orbits of all particles equal to the major radius of the torus. In order to keep all the particles under the torus surface, the eccentricities of their orbits must be in the range $e = [0, r_0]$ and the inclinations, measured from the symmetry plane of the torus, must satisfy the following condition:

$$i = \arcsin \left(q \frac{e}{\sqrt{1-e^2}} \right), \quad (1)$$

where q is a parameter allowing us to change the ellipticity of the torus cross-section. Let $\rho = \sqrt{x^2 + y^2}/R$ be the radial coordinate of a particle in the torus plane of symmetry, measured from the central mass and normalized to R . Then the coordinates of the inner and outer boundaries of the

¹ Note that in Section 4 we will pass from test particles to more realistic objects that have sizes and masses. Therefore collisions between particles will be taken into account.

torus are determined by the eccentricity of the orbit $\rho_{min} = 1 - e$ and $\rho_{max} = 1 + e$. Let us suppose that the argument of perihelion for all orbits $\omega = 0$; that is, the line of nodes coincides with the semi-major axis. We generate randomly the longitude of the ascending node Ω and the true anomaly ν in the range from 0 to 2π . Knowing the orbit elements, we can calculate spatial coordinates for each particle using the well-known formulae (Duboshin 1968)

$$(x, y, z) = r \times (\alpha, \beta, \gamma), \quad (2)$$

where

$$\begin{aligned} \alpha &= \cos \Omega \cos \nu - \sin \Omega \sin \nu \cos i \\ \beta &= \sin \Omega \cos \nu + \cos \Omega \sin \nu \cos i \\ \gamma &= \sin \nu \sin i \end{aligned}$$

and the module of the radius vector from the central mass to the particle

$$r = \frac{R(1 - e^2)}{1 + e \cos \nu}. \quad (3)$$

The velocity components of the particles are determined in the following way:

$$\begin{pmatrix} V_x \\ V_y \\ V_z \end{pmatrix} = \frac{I}{p} \left[\begin{pmatrix} \alpha \\ \beta \\ \gamma \end{pmatrix} \cdot e \sin \nu + \begin{pmatrix} \alpha' \\ \beta' \\ \gamma' \end{pmatrix} (1 + e \cos \nu) \right], \quad (4)$$

where

$$(\alpha', \beta', \gamma') = \frac{d}{d\nu}(\alpha, \beta, \gamma),$$

$p = R(1 - e^2)$ is a focal parameter, and $I = \sqrt{GM_c \cdot p}$ is a module of the kinetic moment. Thereafter, we will use the system in which $G = R = M_c = 1$. Since $R = 1$, the value of the geometrical parameter r_0 uniquely determines the minor radius of the torus and consequently its geometrical thickness. Finally, an algorithm to simulate Keplerian torus is the following.

1. Set the number of particles N , the geometrical parameter r_0 and the ellipticity of the torus cross-section q .
2. Generate randomly the eccentricities within the given limits $e = [0, r_0]$ for each particle and find corresponding values for the inclinations by the formula (1). Also generate Ω and ν randomly for these orbits.
3. Find the spatial coordinates and velocity components by elements of the orbits according to (2) - (4) and use them as the initial values.
4. Solve the equations of motion with the obtained initial conditions ².

Because the investigated system is symmetric with respect to azimuthal angle, it is convenient to use a comoving system of coordinates. This system of coordinates is formed by a plane perpendicular to the plane of torus symmetry and passing through the radius vector of a particle. Thus, one axis of this system ρ coincides with a projection of the radius vector of a particle on the plane of torus symmetry, while second one $\zeta = z/R$ coincides with the axis of torus symmetry. Because a particle is orbiting around the central

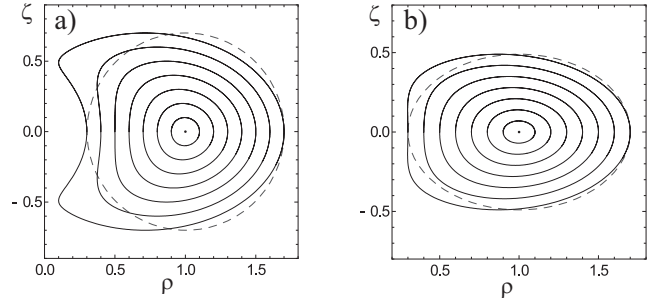


Figure 2. Trajectories of particles with the eccentricities $e = 0.1k$ ($k = 1..7$) in a comoving system of coordinates: a) $q = 1$, b) $q = 0.7$. The central mass is located at the point with coordinates $(0, 0)$. Dashed lines show the circular (a) and elliptical (b) cross-sections. For the limiting case of a thick torus (outer solid curves), the cross-sections of a Keplerian torus differ noticeably from the corresponding circular (a) or elliptical (b) ones.

mass, the comoving system is also orbiting with a velocity equal to the orbital velocity of the particle. The comoving system of coordinates is convenient because the trajectories of particles in this system reflect the shape of the torus cross-section.

The equation of a particle trajectory in the comoving system of coordinates for the case of a Keplerian torus has the following parametric form:

$$\rho = \frac{1 - e^2}{1 + e \cos \nu} \sqrt{1 - q^2 \frac{e^2}{1 - e^2} \sin^2 \nu} \quad (5)$$

$$\zeta = qe \sqrt{1 - e^2} \frac{\sin \nu}{1 + e \cos \nu}. \quad (6)$$

The trajectories of the particles in the comoving system of coordinates calculated with (5) - (6) are presented in Fig 2. The shape of each orbit determines the shape of the cross-section of the torus with a given value of r_0 . The period of a particle in comoving system of coordinates equals the orbital period. Furthermore, the periods of all particles are equal because the semi-major axes of all orbits equal unity ($R = 1$).

It is seen from Fig.2 that the cross-section of the Keplerian torus is different from the circular cross-section for large values of orbit inclinations (the outer trajectories in Fig.2). At small inclinations, the trajectories are nearly circular (inner curves in Fig.2a). Interestingly, the trajectories at large inclinations make the cross-section of the torus a more complicated shape with two humps (Fig.2a). The restriction on the geometrical thickness of a Keplerian torus follows from (1). Indeed, because $\sin i \leq 1$ we obtain the maximum value of the eccentricity $e_{max} = 1/\sqrt{q^2 + 1}$ from (1) which is the upper restriction on r_0 . For $q = 1$, the highest possible value of the geometrical parameter of a Keplerian torus is $r_0 = 1/\sqrt{2} \approx 0.7$. This limit corresponds to the maximum value of orbit inclination $i = \pi/2$; that is, the outer particle is moving in the plane perpendicular to the torus plane of symmetry in this case. Note that if the eccentricities and the inclinations of the orbits of all particles tend to zero, then the Keplerian torus degenerates to an infinitely thin ring. Obviously, because this torus is formed from test particles (interaction between particles is not accounted for), the orbits of the particles are

² The results in the form of animations are presented at <http://astrodata.univer.kharkov.ua/agn/torus/>

always closed and the Keplerian torus is stable.³ This is a limiting case for a self-gravitating torus when its mass tends to zero. In reality, the torus has a mass, and, consequently, one needs to account for its gravitational potential. In the next section we will investigate the trajectories of a test particle in the gravitational potential of the central mass and a homogeneous circular torus.

3 TRAJECTORIES OF TEST PARTICLE IN THE INNER POTENTIAL OF A HOMOGENEOUS CIRCULAR TORUS AND THE CENTRAL MASS

Consider the motion of a test particle in the inner gravitational potential of both the torus and the central mass. Because the expression for the torus potential is not integrable explicitly, we can take advantage of its expansion for the analysis of particle trajectories. Bannikova, Vakulik & Shulga (2011) obtained an approximate expression for the inner gravitational potential of the homogeneous circular torus in the form of a power series up to second-order terms:

$$\varphi_{torus}^{inner}(\eta, \zeta; r_0) \approx \frac{GM_{torus}}{2\pi R} \left[c + a_1 \frac{\eta}{r_0} + a_2 \left(\frac{\eta}{r_0} \right)^2 + b_2 \left(\frac{\zeta}{r_0} \right)^2 \right] \quad (7)$$

where M_{torus} is the torus mass, η , ζ are dimensionless coordinates ($\eta = \rho - 1$) and the coefficients depend on the geometrical parameter r_0 :

$$a_1 = 8k(1 + \ln k), \quad k \equiv r_0/8 \\ a_2 = -1 - 4k^2(11 + 10 \ln k), \quad b_2 = -1 + 4k^2(3 + 2 \ln k).$$

The approximate expression (7) describes the inner potential of a homogeneous circular torus with good accuracy up to $r_0 = 0.5$ and allows to perform a qualitative analysis of the trajectories in the gravitational system "torus + central mass". The coefficient a_1 defines a shift of the potential maximum with respect to the centre of the torus cross-section and the coefficients a_2, b_2 are related to the deviation of the torus potential from quadratic law. As noted in a previous work (Bannikova, Vakulik & Shulga 2011), the inner potential of the torus can be represented as the sum of a cylinder potential and a term comprising the curvature of the torus surface $\varphi(r) = \varphi_{cyl} + \varphi_{curv}$. Two types of central fields are known in which all trajectories of finite motions are closed: $\varphi(r) \propto 1/r$ and $\varphi \propto r^2$ (Landau & Lifshitz 1988). Obviously, closed orbits are possible in the cylinder because its gravitational potential is $\varphi_{cyl} \propto r^2$. However, the presence of a potential of curvature φ_{curv} brings to forming open and more complex orbits of the particle in the inner potential of the torus. We investigate this problem in detail. For the qualitative analysis of particle trajectories in the inner region of the torus, we restrict ourselves to the case of a torus with circular cross-section and homogeneous density distribution. Since the potential of the considered system is axisymmetric, the projection of the angular moment of the particle on axis ζ is a constant value ($I_\zeta = Const$). In

this case, it is convenient to introduce an effective potential (Binney & Tremaine 1994):

$$\varphi_{eff} = \varphi_{torus}^{inner} + \varphi_c - \frac{I_\zeta^2}{2(\eta + 1)^2}, \quad (8)$$

where the potential of the central mass M_c

$$\varphi_c = \frac{GM_c}{R} \frac{1}{\sqrt{(\eta + 1)^2 + \zeta^2}}. \quad (9)$$

We can represent φ_{eff} in the form of a power series up to second-order terms:

$$\varphi_{eff}(\eta, \zeta; r_0) \approx \frac{GM_{torus}}{2\pi R} \left[\tilde{c} + \tilde{a}_1 \frac{\eta}{r_0} + \tilde{a}_2 \left(\frac{\eta}{r_0} \right)^2 + \tilde{b}_2 \left(\frac{\zeta}{r_0} \right)^2 \right], \quad (10)$$

where the coefficients

$$\tilde{c} = 2\pi\mu(2 - l^2) + c \\ \tilde{a}_1 = 2\pi\mu r_0(2 - l^2) + a_1 \\ \tilde{a}_2 = -\pi\mu r_0^2(3l^2 - 2) + a_2 \\ \tilde{b}_2 = -\pi\mu r_0^2 + b_2$$

$\mu = M_c/M_{torus}$ is the ratio of the central mass to the torus mass, and the dimensionless parameter l defines a fraction of the angular momentum from the Keplerian value $I_\zeta^2 = l^2 GM_c/R$. It was shown in (Bannikova, Vakulik & Shulga 2011) that the maximum of the potential of the homogeneous circular torus is displaced inside from the centre of its cross-section. As a result, the torus must be compressed along the major radius. To prevent this compression, an orbital motion is necessary: the gravitational force tending to compress the torus along the major radius is compensated by the centrifugal force. This corresponds to a shift of the maximum of the effective potential to the centre of the torus cross-section; that is, $\tilde{a}_1 = 0$ in (10), whence it follows a condition on the coefficient of the angular momentum:

$$l^2 = 1 - a_1/(2\pi\mu r_0). \quad (11)$$

The equations of a particle trajectory in the comoving system of coordinates can be obtained by solving the equations of motion:

$$\ddot{\eta} \equiv \frac{d^2\eta}{dt^2} = \frac{1}{R} \frac{\partial\varphi_{eff}}{\partial\eta}; \quad \ddot{\zeta} \equiv \frac{d^2\zeta}{dt^2} = \frac{1}{R} \frac{\partial\varphi_{eff}}{\partial\zeta}. \quad (12)$$

These equations have the form of a harmonic oscillator:

$$\ddot{\eta} + \omega_A^2 \eta = 0, \quad \ddot{\zeta} + \omega_B^2 \zeta = 0. \quad (13)$$

Then the solution of the equation (13) can be presented in parametric form:

$$\eta(t) = \eta_0 \cos[\omega_A \cdot t + \alpha], \\ \zeta(t) = \zeta_0 \cos[\omega_B \cdot t + \beta], \quad (14)$$

where η_0, ζ_0 are the coordinates of the particle at initial time, and

$$\omega_A^2 = \frac{GM_{torus}}{\pi R^3 r_0^2} [\pi\mu r_0^2(3l^2 - 2) - a_2], \quad (15)$$

$$\omega_B^2 = \frac{GM_{torus}}{\pi R^3 r_0^2} [\pi\mu r_0^2 - b_2]. \quad (16)$$

Thus, the coordinates of the particle (14) evolve like the displacements of two harmonic oscillators with the epicycle

³ Because there is an analytical solution for $\mathbf{r}(\nu)$ in case of a Keplerian torus we use it as the initial condition in the N -body simulation (Section 4).

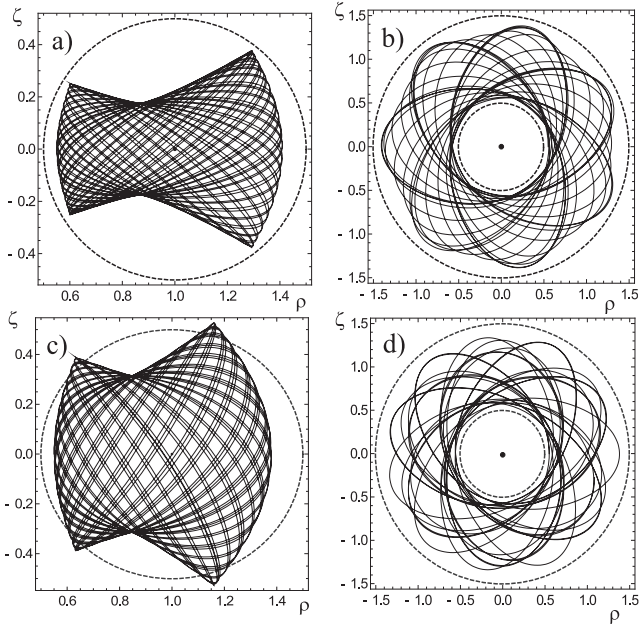


Figure 3. Trajectories of a test particle in the inner potential of homogeneous circular torus and the potential of the central mass. Left column: the trajectory in the comoving system of coordinate for a) $V_\zeta = 0.4$; $l = 0.95$, c) $V_\zeta = 0.7$; $l = 0.90$. The centre of the torus cross-section is marked with a point. Right column: projection of the trajectory on the torus plane of symmetry for b) $V_\zeta = 0.4$; $l = 0.95$; d) $V_\zeta = 0.7$; $l = 0.90$. Dashed lines correspond to edges of the torus cross-section. For all cases $\mu = 1$, $r_0 = 0.5$, $G = R = 1$, $t = 150$.

ω_A and vertical ω_B frequencies, respectively. In this case the orbit is open and the trajectory in the comoving system of coordinates fills some rectangular region during a period P_{box} whereupon this process is repeated. These orbits are known as box orbits (Binney & Tremaine 1994). It is seen from (11) that for $\mu r_0 \gg 1$ the coefficient of angular momentum $l \rightarrow 1$ and the ratio of epicycle frequency ω_A to vertical frequency ω_B takes the form:

$$f \equiv \frac{\omega_A}{\omega_B} = \sqrt{\frac{\pi \mu r_0^2 - a_2}{\pi \mu r_0^2 - b_2}}. \quad (17)$$

Then, the period of a box orbit, expressed in orbital periods, is determined by the expression $P_{box} = 1/|1 - f|$. For $r_0 = 0.3$ and $\mu = 50; 25; 1/0.06$ we obtain $P_{box} = 213; 113; 80$. In the case of $\mu r_0 \gg 1$ ($l \rightarrow 1$) it is apparent from (17) that $\omega_A \rightarrow \omega_B$. This limiting case corresponds to the case of a Keplerian torus.

Fig.3 presents the trajectories of a test particle in the inner gravitational potential of the homogeneous circular torus and the potential of the central mass. For this we used an expansion for the inner potential of the torus in a power series up to fourth-order terms:

$$\varphi_{torus}^{inner}(\eta, \zeta; r_0) \approx \frac{GM_{torus}}{2\pi R} \left[c + \sum_{j=1} a_j \left(\frac{\eta}{r_0}\right)^j + \sum_{k=1} b_k \left(\frac{\zeta}{r_0}\right)^k + \sum_{j=1} \sum_{k=1} t_{jk} \left(\frac{\eta}{r_0}\right)^j \left(\frac{\zeta}{r_0}\right)^k \right], \quad (18)$$

where the coefficients of the expansion can be found in

(Bannikova, Vakulik & Shulga 2011). In contrast to a square-law potential (7), in this case we consider a more explicit approximation of the inner potential of the torus (18). Therefore, the form of the region bounding the place of the particle in the torus cross-section has more complex shape than (14) (Fig.3a,c). Note that box orbits arise as a result of mistiming of the orbital period of the particle and its period in the comoving system of coordinates. If the torus mass is increased, the orbital period of particles is decreased due to turning the line of nodes. This leads to a shift of the pericentre and, therefore, to the formation of a rosette orbit in the torus plane of symmetry (Fig.3b,d). When the torus mass is decreased, the trajectory in the comoving system of the coordinates fills the box area for a longer time; that is, the period of the box orbit increased in this case.

4 SELF-GRAVITATING TORUS IN THE GRAVITATIONAL FIELD OF A CENTRAL MASS: *N*-BODY SIMULATION

This section is devoted to an investigation of a self-gravitating torus located in the field of a central mass. We restrict ourselves to the case of a torus whose mass is up to 10 per cent of the central mass. As the initial condition we use a Keplerian torus (Section 2). We investigate the following main questions:

1. Are the tori stable on time scales comparable to the lifetimes of astrophysical objects?
2. What is the shape of the cross-section of a torus in an equilibrium state?
3. What is the density distribution of particles in the equilibrium state of the torus?

As will be seen below, the self-gravitation significantly changes the cross-section shape of the torus as compared with the case of a Keplerian torus. The gravitational potential of a torus with mass M_{torus} , composed of N gravitating particles of equal masses, at an arbitrary point $\mathbf{r}(\rho, \lambda, \zeta)$ has the form

$$\varphi_{toru}(\rho, \lambda, \zeta) = \frac{GM_{torus}}{R} \sum_{i=1}^N \frac{1}{|\mathbf{r} - \mathbf{r}_i|}, \quad (19)$$

where $\mathbf{r}(\rho, \lambda, \zeta)$ is the dimensionless radius vector of i -th particle normalized to the major radius of the torus R . Taking into account the gravitational interaction of particles forming the torus, the forces acting on a particle can be represented as the sum of regular and irregular components. The regular component is associated with a 'smoothed' potential, and irregular one appears because of the direct gravitational interaction between nearest particles. The role of the irregular forces increases in the case of a relatively small number of the particles. Therefore, the torus potential can be represented as follows:

$$\varphi_{torus}(\rho, \lambda, \zeta) = \varphi_{torus}^{reg}(\rho, \zeta) + \varphi_{torus}^{irr}(\rho, \lambda, \zeta), \quad (20)$$

where the first term is the regular part of the torus potential that is independent on the azimuth angle λ , while the second term is an irregular (random) part of the potential defined

by

$$\varphi_{torus}^{irr}(\rho, \lambda, \zeta) = \frac{G}{R} \left[M_{torus} \sum_{i=1}^N \frac{1}{|\mathbf{r} - \mathbf{r}_i|} - \int_V \frac{\kappa(\mathbf{r}') d\mathbf{V}'}{|\mathbf{r} - \mathbf{r}'|} \right]. \quad (21)$$

Here $\kappa(\mathbf{r})$ is the volume density of the torus. Accounting for the central mass leads to the following expression for the full potential:

$$\varphi(\rho, \lambda, \zeta) = \varphi_c(\rho, \zeta) + \varphi_{torus}(\rho, \lambda, \zeta), \quad (22)$$

where the potential of the central mass is defined by expression (9). The limiting case $\varphi_{torus}^{irr} \rightarrow 0$ (neglecting interactions between particles) corresponds to the problem of the motion of a test particle in the regular gravitational potential of the torus. This problem was analyzed in detail in the approximation of a homogeneous circular torus (Section 3), where it was shown that the trajectories of particles in the cross-section of the torus relates to the type of box orbits. In the following, we will show that the role of the regular part of the potential appears in changing the sizes of the torus cross-section for N -body simulation. On average (by averaging over all i -indices), $\varphi_{torus}^{irr} \rightarrow 0$, but at any particular point φ_{torus}^{irr} can vary considerably from zero, taking both positive and negative values. As a consequence, the velocity of particles moving in the regular potential of the torus will be subject to random perturbations owing to the forces determined by the irregular part of the potential. As a measure of the irregular part of the potential we choose a potential created by a particle at a distance $\tilde{l} = \sqrt[3]{V_{torus}/N}$ equal to the average distance between particles: $\varphi_i = Gm_i/\tilde{l}$. The masses of all particles are the same ($m_i = M_{torus}/N$), and therefore $\varphi_i \propto N^{-2/3}$; that is, the irregular forces become significant for a relatively small number of particles N .

The considered N -body problem is reduced to the numerical integration of the equations of motion taking account of the central mass:

$$\mathbf{a}_i = -\frac{GM_c}{R^2} \frac{\mathbf{r}_i}{r_i^3} + \frac{\mathbf{F}_i}{m_i} \quad (23)$$

where \mathbf{a}_i is the acceleration of i -th particle. The total gravitational force acting on i -th particle is

$$\mathbf{F}_i = -\frac{Gm_i}{R^2} \sum_{j=1}^N m_j \frac{\mathbf{r}_i - \mathbf{r}_j}{(|\mathbf{r}_i - \mathbf{r}_j|^2 + \varepsilon^2)^{3/2}}, \quad (24)$$

where ε is a parameter allowing us to avoid the infinite increase of the force of interaction between two particles when they come close together (Aarseth 1963, 2003). However, the introduction of this parameter means that we simulate not point particles but the mega-particles of spherical form with dimensionless radius ε in which the density distribution obeys Plummer's law (Plummer 1911; Saslaw 1985). In the following numerical simulations we take the parameter $\varepsilon = 0.01$. Note that the clouds penetrate through each other for collisions in this case.

A considerable amount of computer time is needed for the numerical simulation of a system consisting of large numbers of particles and accounting for their gravitational interaction. In this research we used the technology of parallel computing *CUDA* developed by Nvidia, which allows us to significantly reduce the computation time by using the computing resources of graphics processing units

(GPUs). This technology is especially effective for N -body problems (Belleman, Bédorf & Portegies Zwart 2008). The numerical simulation was performed using the graphics card NVIDIA GeForce GTS 250 (192 *CUDA* Cores). The calculation time was about 2 hours for a system of 8 192 particles orbiting over 1000 periods with time step equal 1/150 of the period.

Our main idea is that a torus should be more stable if it is formed by clouds moving in inclined orbits around the central mass. Therefore we use the Keplerian torus of the given geometric parameter r_0 (Section 2) as the initial condition. The solution for a Keplerian torus allows us to calculate the initial coordinates and velocities of particles with inclined orbits. The absence of quasi-periodic fluctuations of macro-parameters of a statistical system is a necessary condition for a system of particles to achieve a quasi-steady state. In order to test this condition, we control the values of the kinetic energy, potential energy and total energy of the system a few times over the period. In addition, in order to control the dynamics of the system, the statistical macro-parameters of the system of particles were recorded with the same frequency, namely the coordinates of the centre of the torus mass in its cross-section (η_c, ζ_c) as well as the effective sizes of the torus cross-section, which were calculated by the following expressions

$$r_\eta = 2\sqrt{\frac{1}{N} \sum_{i=1}^N (\eta_i - \eta_c)^2}, \quad r_\zeta = 2\sqrt{\frac{1}{N} \sum_{i=1}^N (\zeta_i - \zeta_c)^2}, \quad (25)$$

where r_η, r_ζ are respectively the horizontal and the vertical sizes and the 'average' effective size of the cross-section:

$$r_a = \sqrt{(r_\eta^2 + r_\zeta^2)/2}. \quad (26)$$

Note that in the case of a homogeneous circular disc all the effective sizes, defined in such a way, are equal to the geometrical radius of the disc. The angular momentum of the system of particles in the comoving system of coordinates is defined by the expression

$$I_\theta = \sum_{i=1}^N (\eta_i \dot{\zeta}_i - \zeta_i \dot{\eta}_i), \quad (27)$$

where the dot denotes a time derivative. Hereafter, this angular momentum (27) is referred as the 'fictitious' angular momentum. An analysis of the behavior of the fictitious momentum allows us to determine the degree of order (or chaos) of directions of particles movement in the torus cross-section. Furthermore, we periodically register the position (coordinates) of all particles in the plane of the torus cross-section. The accumulation of these positions during each 10 orbital periods allowed us to obtain the average density distribution of particles in the torus cross-section and to analyze the change of cross-section shape during the simulation. The evolution of the torus cross-section during the simulation for different r_0 is presented in the form of an animation at <http://astrodata.univer.kharkov.ua/agn/torus>.

The simulation shows that large changes of kinetic and potential energy take place at the initial stage, $t < 20$ (Fig.4), with the total energy conserved. The change of potential energy is related to the change of shape of the torus cross-section and to the density of particles in it. Just

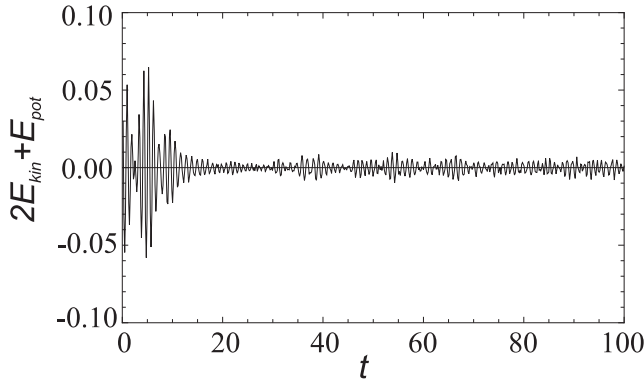


Figure 4. The sum of twice the kinetic and the potential energy of system, $2E_{kin} + E_{pot}$, during the first 100 orbital periods for $M_{torus}/M_c = 0.02$ and $N = 8\,192$. Initial conditions correspond to a Keplerian torus with $r_0 = 0.3$.

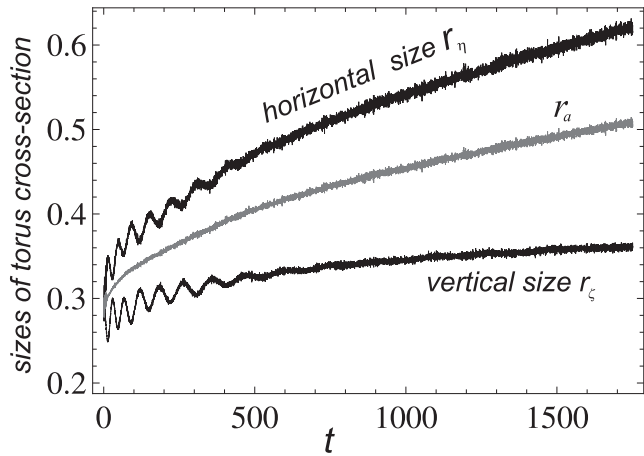


Figure 5. Variation of cross-section sizes of a torus with mass $M_{torus} = 0.02M_c$, consisting of $N = 8\,192$ particles, during 1 800 orbital periods. The initial conditions correspond to a Keplerian torus with $r_0 = 0.3$.

in this short initial time interval, the distribution of particles in the torus varies significantly, and the torus acquires an equilibrium cross-section of oval shape. Furthermore, the sharper part of the oval cross-section is directed to the central mass, and the more flattened part to the outer region. This is the opposite to the situation in the initial state (Keplerian torus). Obviously, the significant fluctuations in energy occur because of the tendency of the torus to acquire a cross-section shape inverted with respect to the initial one. For $t > 20$, the fluctuations of the kinetic and potential energy are negligible. This means that the shape of the torus cross-section does not change significantly anymore. We define this state in which the shape of the torus cross-section is no longer changing as the equilibrium state. Fig. 4 shows that the virial theorem is satisfied, namely $2E_{kin} + E_{pot} \approx 0$, which characterizes the stationary or linearly non-stationary state of the system. Fig.5 shows that the torus cross-section gradually increases with time. The gradual spread of the cross-section is related to the irregular forces arising from the gravitational interaction between particles. Indeed, the irregular forces dominate over the regular ones caused by the smoothed potential for the considered case of a ‘light’

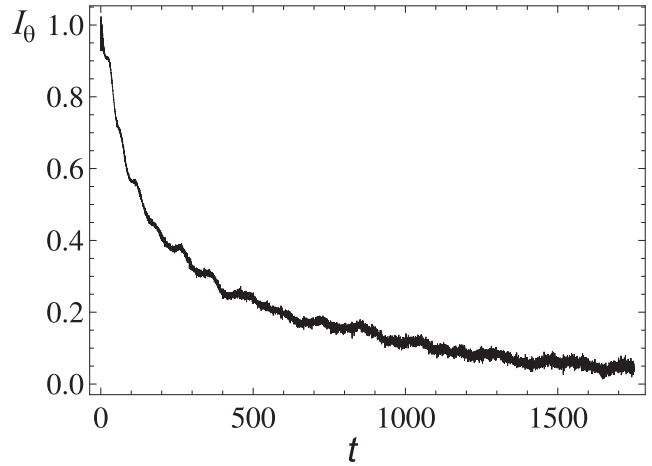


Figure 6. Variation of the fictitious angular momentum for a torus with mass $M_{torus} = 0.02M_c$ and $N = 8\,192$ during 1 800 orbital periods. I_θ is normalized to the initial value that corresponds to a Keplerian torus with $r_0 = 0.3$.

torus ($M_{torus}/M_c = 0.02$). The periodic fluctuations in size (Fig.5) are related to the regular potential of the torus. It was shown in Section 3 that the orbit of a test particle in the inner potential of a circular torus in the comoving coordinate system is of the box-orbit type. In the case of N -particles the box orbits are synchronized at the initial stage, which causes periodic fluctuations of the cross-section of the torus (Fig.5). The amplitude of these oscillations decreases at later stages because of the mistiming of the box orbits. As a consequence, the fictitious angular momentum in the comoving coordinate system, I_θ , also decreases (Fig.6). The system tends to a state with $I_\theta \rightarrow 0$, that is to the randomization the movement directions of particles in the torus cross-section. Note that the total angular momentum of the system is conserved. The changes of sizes of the torus cross-section for a larger value of the initial geometrical parameter, $r_0 = 0.7$, are presented in Fig.7. The significant difference from the previous case of a torus with the smaller initial value $r_0 = 0.3$ is obvious (Fig.5). Namely, the sizes of the cross-section change considerably during the initial time, which is connected to a significant change in the shape of the torus cross-section. Subsequently, the amplitude of the fluctuations decreases and finally disappears after $t = 300$. This behavior can be explained as follows. In the case of a thick torus, the periods of box orbits in the initial stage are very different, which leads to a rapid mistiming of orbits in the torus cross-section. This confirms the analysis of change in the fictitious angular momentum (Fig.8). Thus, the cross-section of a self-gravitating torus spreads slowly (here with the vertical size increasing more slowly than the horizontal one). In the equilibrium state, the directions of particle movements in the torus cross-section are randomized. Note that if the central mass $M_c = 10^7 M_\odot$ then one orbital period ($t = 1$) in the centre of the cross-section of a torus with the major radius $R = 2pc$ correspond to an average interval of 80 000 years (see Section 5). Thus, the results of numerical simulation for $N = 8\,192$ (Figs.5-8) for a time interval of 1 700 orbital periods correspond to 136 million years.

When particles interact with each other, some of them

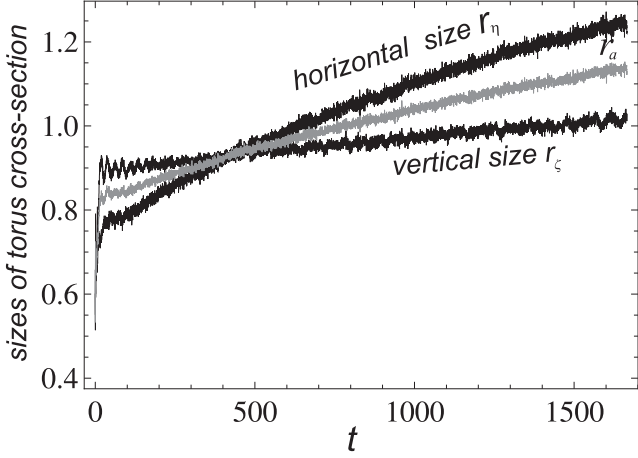


Figure 7. Variation of cross-section sizes of a torus with mass $M_{torus} = 0.109M_c$, consisting of $N = 8\,192$ particles, during 1 800 orbital periods. The initial conditions correspond to a Keplerian torus with $r_0 = 0.7$.

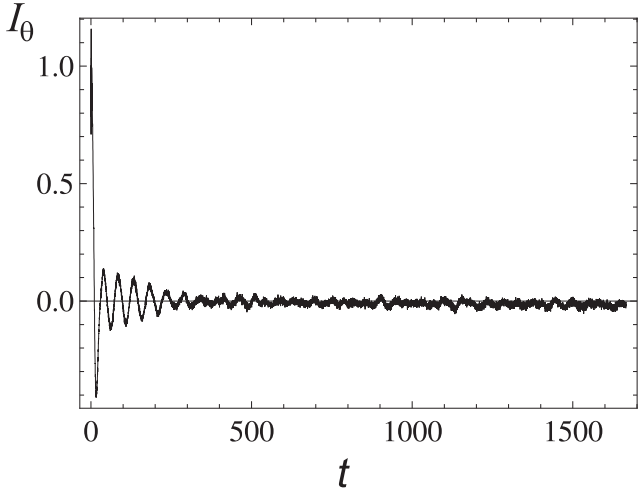


Figure 8. Variation of fictitious angular momentum for a torus with mass $M_{torus} = 0.109M_c$ and $N = 8192$ during 1800 orbital periods. I_θ is normalized to the initial value that corresponds to a Keplerian torus with $r_0 = 0.7$.

lose energy and move to lower orbits, while the energy of other particles increases and they shift to more distant orbits or even escape the system. As a result of such interactions, the outer boundary of the torus cross-section gradually increases. By virtue of the random nature of particle interactions we can assume that the modulus of the total change of a particle velocity ΔV is related to velocity changes in separate encounters of particles ΔV_i as

$$(\Delta V)^2 = \sum_i (\Delta V_i)^2. \quad (28)$$

In the theory of stellar dynamics there is well-known expression for an estimate of the velocity dispersion $(\Delta V)^2$ reached during the interval Δt (Kulikovskii 1978, Saslaw 1985):

$$(\Delta V)^2 = 32\pi G m^2 \Delta t \cdot D \left(\frac{1}{V} \right) \ln \left(\frac{b_{max}}{B} \right), \quad (29)$$

where m is mass of a particle, D is number of particles per unit volume, which for a homogeneous distribution is proportional to N . Omitting the constant coefficients and assuming that the mass of particles $m = M_{torus}/N$, the expression (29) takes the form

$$(\Delta V)^2 \propto G \frac{M_{torus}^2}{N} \Delta t \ln \left(\frac{b_{max}}{B} \right). \quad (30)$$

As an estimate of the maximum impact parameter b_{max} , the average distance \bar{l} between particles is commonly used. Then, the expression for the impact parameter is

$$b_{max} \approx \bar{l} = \sqrt[3]{\frac{2\pi^2 R^3 r_0^2}{N}} \quad (31)$$

and

$$B = \frac{2GM_{torus}}{NV^2}. \quad (32)$$

In the considered dimensionless system we obtain the estimate

$$\ln \left(\frac{b_{max}}{B} \right) \approx \ln \left(\frac{N^{2/3}}{M_{torus}^2} \right). \quad (33)$$

Neglecting the weak logarithmic dependence $(\Delta V)^2$ of N and M_{torus} we finally obtain

$$(\Delta V)^2 \sim M_{torus}^2 \frac{\Delta t}{N}. \quad (34)$$

Although the expression (34) was obtained for a simply connected system of particles, it works satisfactorily in the case of a torus, which is confirmed by results of simulation. For example, if N_1 is number of particles in the torus and Δt_1 is interval during which a certain value of the velocity dispersion is reached, then it follows from (34) that $\Delta t_2 = \Delta t_1 \cdot N_2/N_1$; that is, the same value of the velocity dispersion for $N_2 = N_1/2$ will be reached during $\Delta t_2 = \Delta t_1/2$. Variations of cross-section sizes for tori with different numbers of particles are shown in Fig.9. Black curves were obtained from simulation of a torus with $N_1 = 16\,384$ for the interval $t_1 = 3000$. The gray curves correspond to the torus that consist of $N_2 = N_1/2 = 8\,192$ particles for interval $\Delta t_2 = \Delta t_1/2 = 1\,500$ with subsequent expansion of the obtained curves by a factor of two. The black and gray curves coincide well, which indicates that the expression (34) is satisfactory. *Thus, provided we obtain results of the simulation of the system with a smaller number of particles in a relatively short time interval, expression (34) allows us to predict the state of the system consisting of a larger number of particles for larger time intervals. In a similar way, the condition of re-scaling (34) can be used to investigate systems with different values of M_{torus} .*

We discovered from simulations that in the equilibrium state the torus has an oval cross-section with a density distribution that changes exponentially. The stability of the torus is achieved because the clouds move on inclined orbits. The distribution of particles in the torus cross-section was obtained by averaging their coordinates on the interval of 100 orbital periods with a subsequent approximation by a function of the form

$$n(\eta, \zeta; r_0) = n_0(r_0) \exp[-f(\eta, \zeta; r_0)], \quad (35)$$

where n_0 is the number of particles at a maximum of the distribution. For simplicity we set $n_0 = 1$. Obviously,

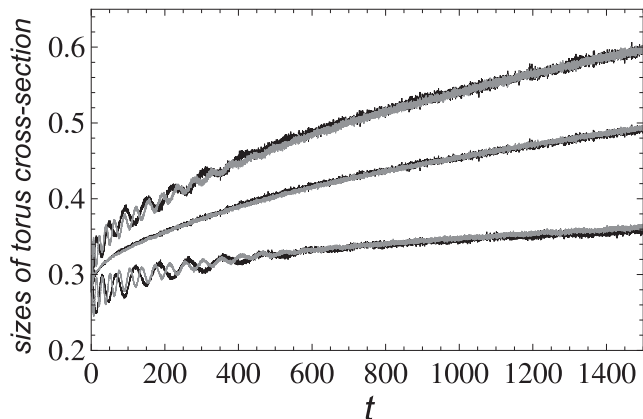


Figure 9. Variation of cross-section sizes of a torus with initial conditions $r_0 = 0.3$, $M_{torus} = 0.02M_c$. The black curves are obtained by simulation with $N_1 = 16\ 384$ for the interval $\Delta t_1 = 3000$. The gray curves correspond to case $N_2 = N_1/2 = 8\ 192$ at $\Delta t_2 = 1\ 500$ with subsequent expansion of the obtained curves by factor of two.

$\ln(n/n_0) = f(\eta, \zeta)$ is equation of an isodense at level n/n_0 for a given density distribution (35). Because the isodenses have an oval shape we approximate the function f as a power series in the coordinates:

$$f(\eta, \zeta) = c + a_1\eta + a_2\eta^2 + b_2\zeta^2 + a_3\eta^3 + t_{12}\eta\zeta^2 + a_4\eta^4 + b_4\zeta^4 + t_{22}\eta^2\zeta^2. \quad (36)$$

Fig.10 shows an average density distributions in the equilibrium cross-section of a torus consisting of $N = 8\ 192$ particles for various values of the torus mass and various initial r_0 . These cross-sections were achieved in 1000 orbital periods. The parameters (M_{torus} and r_0) in Fig.10 are chosen so that in all cases the tori have the same values of the initial volume density: $\kappa_{torus} = M_{torus}/(2\pi^2 R^3 r_0^2) = Const$. We also performed special simulations by changing the initial shape of the torus cross-section. The results of the simulations showed that changes of the initial shape of the torus cross-section (the ellipticity parameter q in (1)) does not substantially influence the equilibrium shape of the cross-section.

So, we come to the following conclusion.

1. *A gravitating torus with mass $\lesssim 0.1M_c$ is stable on time-scales comparable to the lifetimes of the astrophysical objects.*

2. *In the general case, the equilibrium cross-section of the torus has an oval shape. In equilibrium state, the directions of particle movements in the torus cross-section are randomized.*

3. *The density distribution of particles in the torus cross-section obeys Gauss' law with the maximum near to the centre of the cross-section.*

In these simulations we assumed that clouds do not change their shape for close approaches and collisions. Real cloud could significantly change their shape as a result of tidal shearing and collisions. Therefore the question arises: how can orbiting dusty clouds survive for that long time? Krolik & Begelman (1988) considered this problem in detail. They argued that tidal shearing can shred the clouds into smaller pieces. On the other hand, during collisions the material of clouds can be gathered into one giant clump.

A steady state of the clouds can exist if the rates of the two processes are comparable (Krolik & Begelman 1988). Our point is that on average these processes do not change considerably the spread of orbits inclinations. Wind could be an additional source of clouds moving on such orbits: the clumpy wind coming off the accretion disk can feed the torus (Nenkova et al. 2008 Part II). In this case such clouds could acquire inclined orbits.

5 APPLICATION TO THE OBSCURING TORI IN AGN

The obtained results (cross-section shape and density distribution) can be directly applied to the obscuring tori of AGN. We will use the condition of obscuration obtained from analysis of the spectral energy distribution: for total obscuration of the central engine, the number of clouds in the equatorial plane must be greater than 5 (Nenkova et al. 2008 Part I,II).

5.1 Obscuration of the central engine by the torus

Let us find the restrictions on size and number of clouds from a requirement of total obscuration in the equatorial plane. Assuming an optical depth of clouds in the ultraviolet and visible light much greater than unity, we shall consider them as an opaque slab with an area of cross-section $\pi\varepsilon^2 R^2$, where the effective radius of a cloud is $R_{cl} = \varepsilon R$. The volume per one cloud in the case of a circular torus with a homogeneous distribution of density has the form

$$V_N = \frac{V_{torus}}{N} = \frac{2\pi^2 R^3 r_0^2}{N}. \quad (37)$$

We determine the average number of clouds N_s along the line of sight in the equatorial plane of the torus as a product of the number density $1/V_N$ and the volume of a cylinder with the cross-sectional area $\pi\varepsilon^2 R^2$ and cylinder length equals to the diameter of the torus cross-section

$$N_s = \frac{N}{V_{torus}} \pi\varepsilon^2 R^2 2Rr_0 = \frac{N\varepsilon^2}{\pi r_0}. \quad (38)$$

However, the cross-section of a torus affected by self-gravitation takes an oval shape(Fig.10) and the distribution density of the clouds in its cross-section is inhomogeneous (Section 4). Therefore, the expression for the average number of clouds along the line of sight will differ from (38). In this case, the value of the normalization factor n_0 in (35) can be determined from the following condition: the total number of clouds in the torus remains constant when the cross-section of the torus is changed owing to self-gravitation; that is,

$$N = 2\pi n_0 \iint_S dS \exp[-f(\eta, \zeta; r_0)]. \quad (39)$$

Here the integral is taken over an area of torus cross-section S . To obtain the dependence of the number of clouds on the angle θ between the equatorial plane and the line of sight we transform into the polar system of coordinates with the origin at the central mass: $\rho = \eta + 1 = r \cos\theta$, $\zeta =$

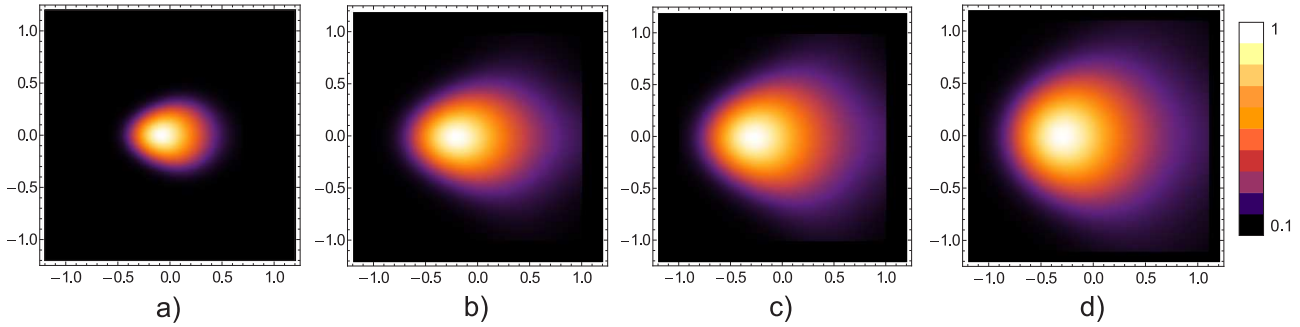


Figure 10. An average density distribution of particles in an equilibrium cross-section of torus consisting of $N=8$ 192 particles for various values of the torus mass and the initial geometrical parameter: a) $r_0 = 0.3$, $M_{torus} = 0.02M_c$, b) $r_0 = 0.5$, $M_{torus} = 0.056M_c$ c) $r_0 = 0.6$, $M_{torus} = 0.08M_c$, d) $r_0 = 0.7$, $M_{torus} = 0.109M_c$. The density distributions are plotted in cylindrical coordinates $(\eta; \zeta)$ and the central mass is at the point with coordinates $(-1, 0)$.

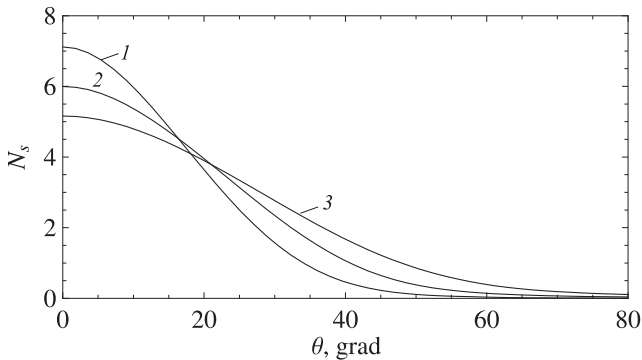


Figure 11. Dependence of the number of clouds along the line of sight on the equatorial angle θ calculated by (40). The different curves correspond to tori with equilibrium cross-sections obtained for different values of the torus mass and the initial geometrical parameter: 1) $r_0 = 0.5$, $M_{torus} = 0.056M_c$ 2) $r_0 = 0.6$, $M_{torus} = 0.08M_c$, 3) $r_0 = 0.7$, $M_{torus} = 0.109M_c$.

The total number of clouds in the torus $N = 10^5$ and $\varepsilon = 0.01$.

$r \sin \theta$. Then the number of clouds along the line of sight as a function of angle is

$$N_s(\theta) = \frac{N\varepsilon^2}{2} \frac{\int_0^\infty e^{-f(r,\theta)} dr}{\iint_S e^{-f(\eta,\zeta)} dS}. \quad (40)$$

Thus, the average number of clouds along the line of sight in the equatorial plane of the torus, taking into account the inhomogeneous distribution of particles (40), is given by:

$$N_s = N_s(0) = \frac{N\varepsilon^2}{2} \frac{\int_0^\infty e^{-f(r,0)} dr}{\iint_S e^{-f(\eta,\zeta)} dS}. \quad (41)$$

For the limiting case of a homogeneous circular torus, the integral in the numerator is equal to $2r_0$ and the integral in the denominator is equal to the area of a circle, and thus the expression (41) reduces to (38). The number of clouds along the line of sight is an important parameter because it characterizes the optical thickness of the torus. Indeed, by virtue of the random distribution of clouds in the torus, the fraction of non-obscured area I_p , which corresponds to the fraction of transmitted radiation of the central engine, is determined by a Poisson distribution $I_p = \text{prob}(k) =$

$N_s^k e^{-N_s}/k!$ with $k = 0$, where k is the frequency of events. Consequently, $I_p = e^{-N_s}$. On the other hand, because $I_p = e^{-\tau_V}$, the optical depth of the torus in visible light equals the average number of clouds: $\tau_V = N_s$. Fig.11 shows the number of clouds along the line of sight as a function of the equatorial angle θ for three cases corresponding the equilibrium cross-sections in Fig.10 b,c,d. In order to fit the observational data, the number of clouds along the line of sight in the equatorial plane of the torus N_s should be greater than 5 (Nenkova et al., part 2, 2008). If $\varepsilon = 0.01$ then this condition holds for a torus with total number of clouds $N = 10^5$ and $r_0 \geq 0.5$. The total number of clouds decreases with the increasing relative size of clouds because $N \propto \varepsilon^{-2}$.

5.2 Dynamics of clouds in the torus

Clouds in the torus are orbiting in the gravitational field of the central mass. Owing the fact that the orbits of clouds have a scatter in eccentricities and inclinations, they form a toroidal structure. Although the orbits are perturbed by mutual attraction of the clouds, the average velocity near the torus plane of symmetry can be determined as the velocity in a circular orbit:

$$V \simeq 210 \text{ km/s} \left(\frac{M_c}{10^7 M_\odot} \right)^{1/2} \left(\frac{r}{1 \text{ pc}} \right)^{-1/2}. \quad (42)$$

Then the orbital period of a cloud can be estimated as

$$P \simeq 30 \text{ 000 year} \cdot \left(\frac{M_c}{10^7 M_\odot} \right)^{-1/2} \left(\frac{r}{1 \text{ pc}} \right)^{3/2}. \quad (43)$$

For the central mass $M_c = 10^7 M_\odot$ the velocity is $V = 150 \text{ km/s}$ at distance $r = 2 \text{ pc}$, and the corresponding orbital period $P \simeq 80000 \text{ year}$. The inner edge of the torus (r_{min}) is formed by clouds that are moving in elliptical orbits and pass through the pericentre, while the outer edge (r_{max}) is formed by clouds that pass through the apocentre. So, the cloud velocities in these two regions can be estimated approximately as:

$$V_{\max} \simeq V_0 \sqrt{\frac{1+r_0}{1-r_0}}, \quad V_{\min} \simeq V_0 \sqrt{\frac{1-r_0}{1+r_0}}, \quad (44)$$

where $V_0 = \sqrt{GM_c/a}$ and $a = (r_{max} + r_{min})/2$ is the semi-major axis. For example if $r_{min} = 0.4 \text{ pc}$ and $r_{max} = 4 \text{ pc}$

the maximum velocity of clouds $V_{\max} \simeq 330\text{km/s}$ and the minimum velocity $V_{\min} \simeq 60\text{km/s}$ for $r_0 = 0.7$.

6 CONCLUSION

In this paper the gravitational properties of a torus have been investigated. It is shown that the presence of a central mass is a necessary condition for the stability of a self-gravitating torus. If the mass of the torus is much lower than the central mass, such a system can be considered in the framework of the problem of test particles motion in the central gravitational field. The toroidal distribution of particles is achieved as a result of the significant spread of inclinations and eccentricities of their orbits. In this case the particles move on Keplerian orbits, and we call a torus formed in this way as 'Keplerian torus'. It is shown that Keplerian torus has a limit on the geometric parameter.

To investigate the properties of a self-gravitating torus we considered the *N*-body problem for a torus located in gravitational field of a central mass. As initial conditions we used the Keplerian torus. It is shown that the self-gravitating torus is stable on time-scale comparable to lifetimes of astrophysical objects. The equilibrium cross-section of the torus has an oval shape with Gaussian density distribution. Until now, the cross-section shape and the distribution of particles in a self-gravitating torus were not known and therefore were taken as free parameters in problems such as radiation transfer in an obscuring torus in AGN. We found the dependence of the obscuring efficiency as a function of the angle between the line of sight and the torus plane of symmetry.

An account of the dissipation processes is a separate issue that is beyond the scope of this paper. The clouds can be heated as a result of collisions, thus creating additional radiation pressure inside the torus. It is likely that these processes can lead to a 'repulsion' of clouds and hence additionally influence at the shape of the torus cross-section.

ACKNOWLEDGMENTS

This work was partly supported by the National Program "CosmoMicroPhysics".

We are grateful to an anonymous referee for the most valuable comments and suggestions, and to Peter Petrov for helpful discussions.

REFERENCES

Aarseth S.J., 1963, MNRAS, 126, 223
 Aarseth S.J. "Gravitational N-Body Simulation: Tools and Algorithms 2003, Cambridge University Press, 430p.
 Antonucci R., 1993, ARA&A, 31, 473
 Bannikova E.Yu., Kontorovich V.M., 2007, Astronomy Reports, 51, 264
 Bannikova E.Yu., Vakulik V.G., Shulga V.M., 2011, MNRAS, 411, 557
 Belleman R.G., Bédorf J., Portegies Zwart S.F., 2008, New Astronomy, 13, 103
 Binney J., & Tremaine S. "Galactic Dynamics 1994, Princeton University Press, Third Printing, 733p.

Dorodnitsyn A., Bisnovaty-Kogan G.S., & Kallman T., ApJ, 2011, 741, 29
 Dorodnitsyn A., Kallman T. & Bisnovaty-Kogan G. S., 2012, ApJ, 747, 8
 Duboshin G.N., "Celestial Mechanics 1968, Moscow, Nauka, 800p. (in Russian)
 Dullemond C.P., & van Bemmell I.M., 2005, A&A, 436, 47
 Elitzur M., & Shlosman I., ApJ, 2006, 648, L101
 Ghez A.M., Salim S., Hornstein S.D., Tanner A., Lu J.R., Morris M., Becklin E.E., and Duchêne G., 2005, ApJ, 620, 744
 Gillessen S., Genzel R., Fritz T.K., Quataert E., Alig C., Burkert A., Cuadra J., Eisenhauer F., Pfuhl O., Dodds-Eden K., Gammie C. F., Ott T., 2012, Nature, 481, 51
 Greenhill L.J., Gwinn C.R., Antonucci R., Barvainis R., 1996, ApJ, 472, L21
 Huré J.-M., 2002, A&A, 395, L21
 Jaffe W. et al., 2004, Nature, 429, 47
 Königl A., & Kartje J.F., ApJ, 1994, 434, 446
 Krolik J.H., & Begelman M.C., 1988, ApJ, 329, 702
 Krolik J.H., 2007, ApJ, 661, 52
 Kulikovskii P.G. "Stellar Astronomy 1978, Moscow, Nauka, 256p. (in Russian)
 Landau L.D., & Lifshitz E.M. Course of Theoretical Physics. Vol.1: "Mechanics 1988, Moscow:Nauka, Fourth Printing, 214c. (in Russian)
 Lodato G., & Bertin G., 2003, A&A, 398, 517
 Nenkova M., Sirocky M.M.; Ivezic Ž.; Elitzur M., 2008, ApJ, 685, 147
 Nenkova M., Sirocky M.M.; Ivezic Ž.; Elitzur M., 2008, ApJ, 685, 160
 Osterbrock D.E. & Shaw R.A., 1988, ApJ, 327, 89
 Pier E.A., & Krolik J.H., 1992, ApJ, 401, 99
 Plummer H. C. 1911, MNRAS, 71, 460
 Raban D., Jaffe W., Rottgering H., Meisenheimer K., Tristram K.R.W., 2009, MNRAS, 394, 1325
 Saslaw W.C. "Gravitational Physics of Stellar and Galactic Systems 1985, Cambridge, Cambridge University Press, 506p.
 Schartmann M., Meisenheimer K., Camenzind M., Wolf S., and Henning T., 2005, A&A, 437, 861
 Schartmann M., Meisenheimer K., Camenzind M., Wolf S., Tristram K. R. W., Henning T., 2008, A&A, 482, 67
 Schartmann M., Burkert A., Krause M., Camenzind M., Meisenheimer K., Davies R.I., 2010, MNRAS, 403, 1801
 Schmitt H.R., Antonucci R.R.J., Ulvestad J.S., Kinney A.L., Clarke C.J., Pringle J.E., 2001, ApJ, 555, 663
 Urry C.M., Padovani P., 1995, PASP, 107, 803
 Wada, K., & Norman, C. A., 2002, ApJ, 566, L21
 Wada K., Papadopoulos P.P., Spaans M., 2009, ApJ, 702, 63
 Weigelt G., Wittkowski M., Balega Y.Y., Beckert T., Duschl W.J., et al. 2004, A&A, 425, 77
 Wittkowski M., Balega Y., Beckert T., et al., 1998, A&A, 329, L45
 Weinberger A.J., Neugebauer G., & Matthews K. 1999, AJ, 117, 2748